



Pseudotachylyte-Mylonites Record of Transient Creep From Inter-Seismic Ductile to Co-Seismic Rupture

Wenhao Dai, Yongsheng Zhou* and Xi Ma

State Key Laboratory of Earthquake Dynamics, Institute of Geology, China Earthquake Administration, Beijing, China

Transient creep during an earthquake cycle is very important to understand the rheology of fault and deformation mechanisms in the brittle–plastic transition zone. In this paper, we analyzed the microstructures of samples for mylonites, *pseudotachylyte*, and *cataclasite* under optical microscope, SEM, and EBSD, which were collected from the Red River fault in southwest of China, where we uncovered a series of ductile to brittle deformed rocks which recorded transient creep related to earthquakes. The results show that mylonites formed at the inter-seismic creep were overprinted by pseudotachylyte and *cataclasite* which were produced during co-seismic rupture, and cracks in *cataclasite* were healed during the post-seismic relaxation. Based on the analysis of the microstructures and deformation mechanism of fault rocks, we propose the oscillation deformation model to explain transient creep of the brittle–plastic transition zone during the seismic cycle in the Red River fault.

Keywords: pseudotachylyte, mylonites, cataclasite, transient creep, earthquake, brittle–plastic transition, Red River fault

OPEN ACCESS

Edited by:

Lidong Dai,

Institute of Geochemistry (CAS), China

Reviewed by:

Qiaomu Qi,

Chengdu University of Technology,
China

Maining Ma,

University of Chinese Academy of
Sciences, China

Xiaoge Huang,

Institute of Geology and Geophysics
(CAS), China

*Correspondence:

Yongsheng Zhou
zhouysh@ies.ac.cn

Specialty section:

This article was submitted to
Solid Earth Geophysics,
a section of the journal
Frontiers in Earth Science

Received: 28 April 2022

Accepted: 10 May 2022

Published: 22 June 2022

Citation:

Dai W, Zhou Y and Ma X (2022)
*Pseudotachylyte-Mylonites Record of
Transient Creep From Inter-Seismic
Ductile to Co-Seismic Rupture.*
Front. Earth Sci. 10:931005.
doi: 10.3389/feart.2022.931005

1 INTRODUCTION

The continental crust has strong rheological layering. The deformation of the upper crust is dominated by brittle deformations of frictional sliding and fractures. In the middle and lower crusts, thermally related dislocation creep is considered to be the main deformation (Brace and Kohlstedt, 1980). The transition from brittle deformation to plastic flow is called as brittle–plastic transition, which is considered as a key layer for determining the depth limit of seismicity in the continental crust (Tse and Rice, 1986; Scholz, 1988).

There are several factors which affect the brittle–plastic transition of crustal rocks, mainly including geothermal gradient, strain rate, mineralogy, structure, fault orientation, and fluid (Sibson, 1983; Tullis and Yund, 1992; Kohlstedt et al., 1995; Montési and Zuber, 2002; Gueydan et al., 2004; Chernak et al., 2009; Ikari et al., 2011). Recent studies show that temperature, strain rate, and pore fluid pressure are the most important factors affecting the deformation of the brittle–plastic transition zone related to the seismic fault during inter-seismic creep, co-seismic loading, and post-seismic relaxation creep (Trepmann and Stöckhert, 2003; Trepmann et al., 2007; Trepmann and Stöckhert, 2013; Trepmann et al., 2017; Dai and Zhou, 2019).

To understand the transient creep of the brittle–plastic transition zone under oscillation conditions of stress and transient strain rate during the earthquake cycle, it is necessary to study in detail the microstructures and deformation mechanism of fault rocks in the deep crust (Campbell and Menegon, 2019). Pseudotachylytes and mylonites in the exhumed mid-to-lower crustal rocks record transient seismic slip, representative of brittle–plastic transition and ductile flow layer

(Sibson, 1980). Mylonite is a type of fault rock in the ductile shear zone formed by plastic deformation. Pseudotachylyte is a solidified melt produced during co-seismic slip along a fault plane in silicate rocks, which represent co-seismic fracture of the epicenter rocks. Most studies reckon that pseudotachylyte is the quenched-phase silicate melt generated after high-velocity friction of fault under dry conditions, recording co-seismic sliding along the fault, which is considered to be an important product of seismic faulting (McKenzie and Brune, 1972; Sibson, 1975; Cowan, 1999; Bestmann et al., 2011; Bestmann et al., 2012). However, pseudotachylyte could also be produced in wet rocks (Song et al., 2020). Several models have been proposed to explain this association of mylonite and pseudotachylyte (White, 2012; Papa et al., 2020).

of the seismogenic crust can propagate downward into the underlying ductile crust (Tse and Rice, 1986), producing pseudotachylytes that are overprinted by mylonitisation during post- and inter-seismic creep (Sibson, 1980; Hobbs et al., 1986; Camacho et al., 1995; White, 1996; Pennacchioni and Cesare, 1997; Lin et al., 2005; Moecher and Steltenpohl, 2009). Some cases revealed that mylonite is produced under a long-term low strain rate and low stress conditions during inter-seismic creep, whereas pseudotachylyte is the result of a short-term high strain rate and high stress deformation by accelerating viscous creep during co-seismic rupture (Trepmann and Stöckhert, 2003; Trepmann et al., 2007; Trepmann and Stöckhert, 2013; Trepmann et al., 2017; Wintsch and Yeh, 2013; Papa et al., 2020).

- 1) Pseudotachylyte formed within ductile deformed rocks. The ductile shear zone is overprinted by pseudotachylyte (White, 2012). Earthquake ruptures nucleating at the base
- 2) Co-seismic crystal-plastic deformation. Mylonites located adjacent to fault melt and associated cataclasis are interpreted to be a result of enhanced ductility arising from

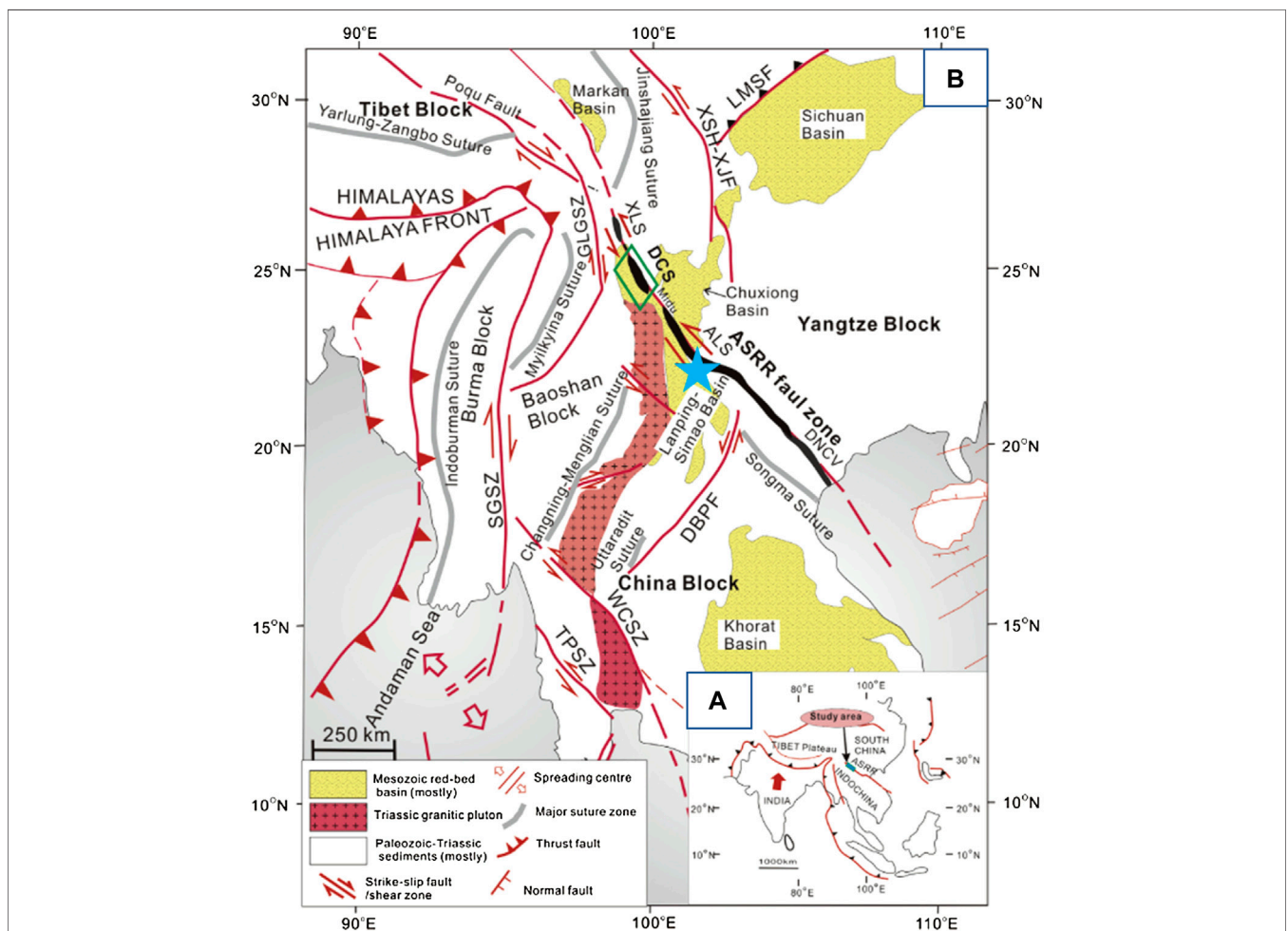


FIGURE 1 | Tectonic sketch map of the Red River fault area (from Cao et al., 2017). **(A)** Simplified geological sketch of the extrusion of Indochina. **(B)** Tectonic sketch map showing the main tectonic zones and the location of the Ailao Shan–Red River (ASRR) shear zone at the eastern margin of the SE. GLGSZ, Gaoligong shear zone; SGSZ, Sagaing shear zone; TPSZ, Three Pagoda shear zone; WCSZ, Wang Chao shear zone; LMSF, Longmen Shan fault; XSH-XJF, Xianshuihe–Xiaojiang faults; DBPF, Dien Bien Phu fault; ASRRSZ, Ailao Shan–Red River shear zone; XLS, Xuelong Shan; DCS, Diancang Shan; ALS, Ailao Shan; DNCV, Day Nui Con Voi; Blue Star, samples location.

the frictionally generated thermal pulse that causes melting (Kim et al., 2010; Bestmann et al., 2011; Bestmann et al., 2012; White, 2012).

- 3) Pseudotachylyte transforms into ultramylonite. Hydration and grain growth within pseudotachylyte layers form ultra-fine-grained rock which can be deformed by grain-size sensitive diffusion creep (Passchier, 1982; White, 1996; Takagi et al., 1999; Pennacchioni et al., 2006; White, 2012).

The mylonite and associated pseudotachylyte from the Red River fault provide an example to study transient creep of the brittle–plastic transition zone during the earthquake cycle. In this study, the microstructures of mylonite, *cataclasite*, and pseudotachylyte collected in the Red River fault zone were analyzed. Based on the deformation characteristics and mechanisms, the oscillation deformation model of inter-seismic creep and co-seismic rupture was determined following the former conception (Trepmann and Stöckhert, 2003; Trepmann et al., 2007; Trepmann and Stöckhert, 2013; Trepmann et al., 2017).

2 GEOLOGICAL SETTING

2.1 Background

The Red River fault (RRF) is a large-scale strike-slip fault in the southeast Asian continent (Molnar and Tapponnier, 1975; Molnar and Tapponnier, 1977; Tapponnier et al., 1982; Tapponnier et al., 1986; Cao et al., 2011a; Cao et al., 2011b; Cao et al., 2012; Cao et al., 2017), which is the consequence of Cenozoic continental collision between the Indian and Eurasian plates since the Eocene (Molnar and Tapponnier, 1977) (**Figure 1A**). Along the RRF zone, the Dianchang Shan and Ailao Shan metamorphic complexes are exposed. The high-grade metamorphic complexes comprise metamorphosed pelitic, mafic, carbonate rocks, and granitic intrusions (Leloup et al., 1995; Liu et al., 2008; Cao et al., 2011a; Cao et al., 2011b; Cao et al., 2012; Cao et al., 2017). These rocks experienced both high-grade metamorphism from upper greenschist to upper amphibolite or granulite facies and high-temperature deformation developing medium to strong foliation (Leloup and Kienast, 1993; Cao et al., 2011a; Cao et al., 2011b; Cao et al., 2012; Cao et al., 2017), which were subsequently sheared at relatively low temperature conditions during late tectonic processes (Cao et al., 2011a; Cao et al., 2011b; Cao et al., 2012; Cao et al., 2017). The ductile shear zone developed in the localized strong deformed zone, and mylonite was formed by high-temperature shear deformation. Pseudotachylyte was found within the local area of the ductile shear zone at Ailao Shan metamorphic complexes (Dai and Zhou, 2019) and Dianchang Shan metamorphic complexes (Li et al., 2022). The deformed metamorphic complexes preserve information on the thermal and tectonic evolution of the RRF fault zone (Leloup et al., 1995; Liu et al., 2006; Cao et al., 2011a; Cao et al., 2011b; Cao et al., 2012). Based on a large number of age data, the ductile deformed granite underwent three stages of cooling history (Wintsch and Yeh, 2013; Cao et al., 2017): quick cooling from 700 to 400°C before

24 Ma, the temperature remaining about 250–350°C with nearly no cooling during the geological period of about 24–5 Ma, and quick upliftment to the ground after 5 Ma. Wintsch and Yeh (2013) suggest that the protolith of granitic rock was deformed to foliated schist and mylonite by dislocation creep at the first cooling stage at a temperature of 400–700°C. However, the deformed granitic rock was overprinted by multiple brittle–plastic deformations during the second cooling period, which includes cataclasis-reaction creep–fracture and K-feldspar vein filling—dissolution creep occurred at 250–350°C (Wintsch and Yeh, 2013). The multiple brittle–plastic–brittle deformations under the similar temperature condition indicates the change of strain rate and pore fluid pressure at the constant depth of crust, which is believed to be related to fault activity during the seismic cycle (Trepmann and Stöckhert, 2003; Trepmann et al., 2007; Trepmann and Stöckhert, 2013; Zhou et al., 2014; Nevitt et al., 2017; Trepmann et al., 2017). Pseudotachylyte found in the ductile shear zone provides direct evidence of co-seismic rupture in geological times.

2.2 Samples

The samples of mylonite (Y11-1A, Y11-1C, Y11-3, and 110827-2), pseudotachylyte (Y11-1B and 110827-3), and cataclasite (Y11-2A, Y11-2B, and Y11-1D) were collected at location of the small valley besides the Qingshuihe Power Station from the Yuanjiang-Mojiang section in the middle segment of the Red River fault zone, and the samples of mylonite (110829-1 and 110829-2) were collected from the section west of Honghe town in the southern segment of the Red River fault zone in Yunnan, China (**Figure 1B**). The sampling locations are in the ductile shear zone developed at the Ailaoshan metamorphic complex.

The mylonite specimens mainly developed the foliation accompanied augen-shaped structure (**Figure 2A**). The elongated σ -type eyeball-like phenocrysts are dominated by feldspar, and the matrix consists of banded quartz, biotite, muscovite, and hornblende, which consists of foliation by plastic flow. Under the microscope, it can be observed that the directional arrangement of minerals constitutes stretching lineation, quartz, and feldspar undulose extinction. The elongated feldspar porphyroclasts and quartz with undulose extinction develop typical core-and-mantle structures.

Pseudotachylyte displays a kind of black vein with a width of about 2–5 cm which appeared within cataclasite and mylonite (**Figures 2B,C**), and the boundary between the pseudotachylyte and the host rock is sharp. The mylonite foliation is obliquely cut by the black veins of pseudotachylyte. The mylonite around the pseudotachylyte underwent brittle fracture to form cataclasite. Cataclasite developed fragmented structures (**Figures 2C,D**). The grinded structure is obvious under the microscope (**Figures 2E,F**), and the cracks are filled with the quartz vein and calcite vein.

3 ANALYTICAL METHODS

All analyses were carried out on oriented samples. Polished XZ-oriented thin sections were prepared by cutting parallel to the

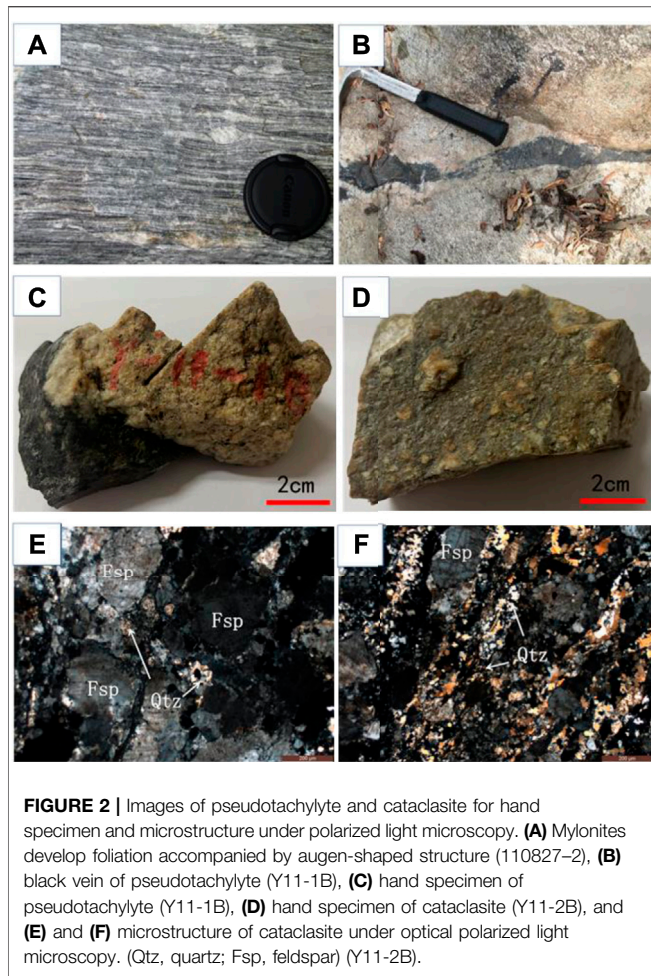


FIGURE 2 | Images of pseudotachylyte and cataclasite for hand specimen and microstructure under polarized light microscopy. (A) Mylonites develop foliation accompanied by augen-shaped structure (110827-2), (B) black vein of pseudotachylyte (Y11-1B), (C) hand specimen of pseudotachylyte (Y11-1B), (D) hand specimen of cataclasite (Y11-2B), and (E) and (F) microstructure of cataclasite under optical polarized light microscopy. (Qtz, quartz; Fsp, feldspar) (Y11-2B).

mineral lineation (X -axis) and perpendicular to the foliation (XY plane) of the mylonites. The microstructures and quartz fabrics were analyzed using an optical microscope (OM), scanning electron microscopy (SEM), and electron backscatter diffraction (EBSD). The chemical composition was analyzed using scanning electron microscopy with energy-dispersive X-ray (EDS).

SEM is an effective instrument to observe the microstructure of rocks. It focuses on observing the spatial relationship between mineral materials by giving a different greyscale contrast, but it cannot measure the crystal orientations of mineral materials. EBSD is a kind of SEM-based technique to measure crystal orientations. It is applicable to any crystalline material (in theory) to provide the absolute crystal orientation with sub-micron resolution. EBSD is a useful tool for discriminating between phases.

The microstructures of mylonite, pseudotachylyte, and cataclasite were observed under SEM, and the quartz fabrics were measured by SEM-EBSD analysis using a Zeiss Sigma scanning electron microscope (SEM) coupled with an Oxford Nordlys nano electron backscattered diffraction (EBSD) detector at the State Key Laboratory of Earthquake Dynamics, Institute of Geology, China Earthquake Administration, Beijing, China.

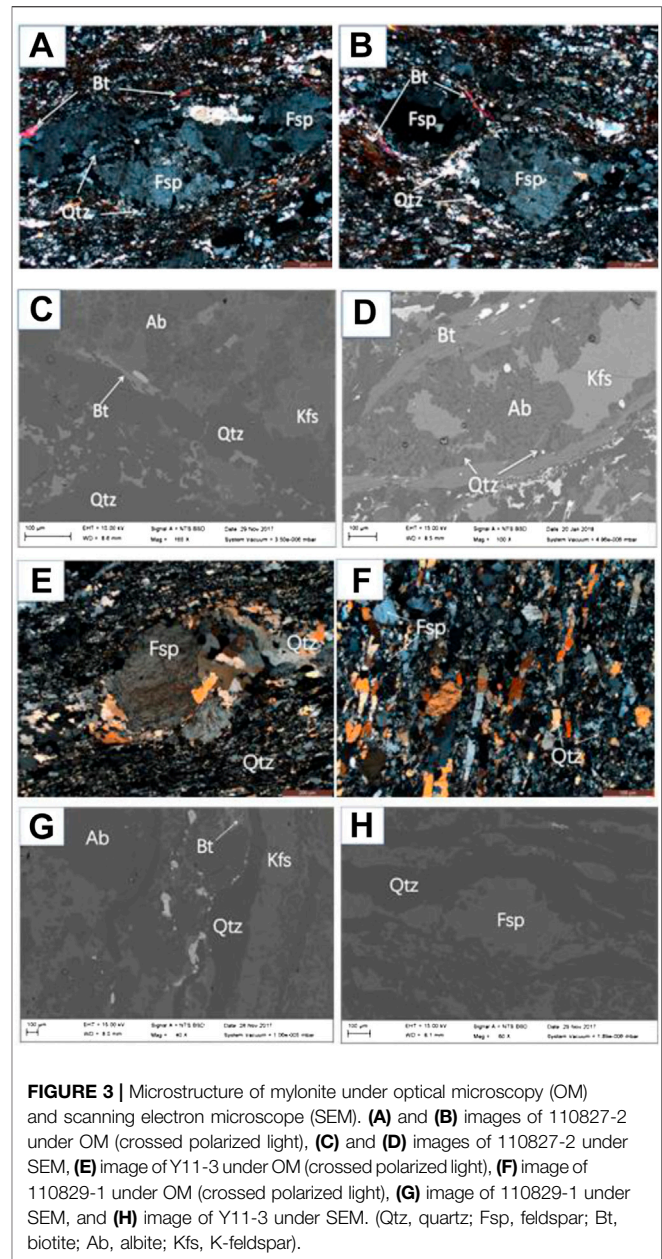


FIGURE 3 | Microstructure of mylonite under optical microscopy (OM) and scanning electron microscope (SEM). (A) and (B) images of 110827-2 under OM (crossed polarized light), (C) and (D) images of 110827-2 under SEM, (E) image of Y11-3 under OM (crossed polarized light), (F) image of 110829-1 under OM (crossed polarized light), (G) image of 110829-1 under SEM, and (H) image of Y11-3 under SEM. (Qtz, quartz; Fsp, feldspar; Bt, biotite; Ab, albite; Kfs, K-feldspar).

Polished thin sections were carbon-coated prior to EBSD analysis. EBSD allows the determination of the full crystallographic orientation of crystals in a thin section using a backscattered electron (BSE) signal. Automatic EBSD measurements were used to obtain orientation maps and crystallographic preferred orientation (CPO) patterns. Working conditions during acquisition of the EBSD patterns were 20 kV accelerating voltage, 12-nA probe current, 70° sample tilt, ~20 mm working distance, and high vacuum. EBSD patterns of quartz were acquired and indexed with AZtec software (Oxford Instruments) which selected the direction of the stretching lineation as the X -axis direction, that is, the quartz-mica strip direction is the X -axis direction and the plane-oriented direction is the XY -plane direction. CHANNEL 5 software (Oxford

Instruments) was used for noise reduction and for filling the missing data with at least eight identical neighbors with similar orientation. All stereographic diagrams of EBSD are lower hemisphere projections.

4 RESULTS

4.1 Mylonite

4.1.1 Microstructures of Plastic Deformation of Mylonite

Sample 110827-2 is a typical fine-grained mylonite. The samples of mylonite (110829-1, 110829-2, Y11-3, Y11-1A, and Y11-1C) contain augen-shaped feldspar porphyroclasts. The microstructures on all six samples were observed, and the deformation characters are similar for all thin sections. Results from three examples (110827-2, Y11-3, and 110829-1) were presented here to show representative deformation behaviors.

The fine-grained mylonite sample 110827-2 was collected from the same section as the pseudotachylyte (Y11-1B and 110827-3). Optical polarized light microscope images show that quartz developed sub-grain textures, feldspar is larger in size than quartz grains, and the grain boundaries are irregular and most edges of the grains became sinuous (**Figures 3A,B**). All of these phenomena show that feldspar and quartz underwent middle temperature deformation of dynamic recrystallization (**Figures 3A,B**). Fine-grained quartz and mica bands constitute the foliation. Mechanical twinned crystals developed in feldspar porphyroclasts which have a crushed structure inside, and the cracks are filled with recrystallized quartz and feldspar (**Figure 3B**). Mica is distributed in the interstices of quartz aggregates which surround the feldspar phenocrysts, showing water–rock reaction at the rims of feldspar (**Figures 3A,B**).

Under the scanning electron microscope, the grains of quartz are elongated and form foliation with mica bands, indicating that the rock has undergone strong plastic deformation (**Figures 3C,D**). The backscattered electron (BSE) images and the EDS analysis show that composition variations of the feldspar due to the dissolution, feldspar porphyroclasts underwent dissolution and decomposition to albite and potassium feldspar (**Figure 3D**).

Sample Y11-3 has a plaque-like structure under an optical polarizing microscope. The boundaries of feldspar phenocrysts are mostly sinuous, with crushed structures, and the matrix is composed of an aggregate of fine-grained feldspar, quartz, and elongated biotite bands, which display the characteristics of plastic flow (**Figure 3E**). Fine-grained quartz and mica aggregates are accumulated on both sides of the trailing tail of the ocular feldspar phenocryst and biotite distributed between the quartz grains or around the edge of the feldspar (**Figure 3E**), indicating that the feldspar has undergone pressure solution. Quartz has a semi-automorphic shape with developed sub-grains and bulging texture at the grain boundaries (**Figure 3E**). The boundaries of feldspar grains in the matrix are bulged, and all of these characteristics indicate that the fine-grained feldspar, quartz, and biotite have undergone low-temperature dislocation creep. It can be seen under the scanning electron

micrograph that quartz bands are thin and feldspar bands are thick, and feldspar bands are cut and intersected by the quartz bands (**Figure 3G**).

Sample 110829-1 has an augen-shaped structure under an optical polarizing microscope. The phenocryst of feldspar is automorphic or semi-automorphic. The boundaries are irregular and sinuous, and some feldspars develop cracks (**Figure 3F**). The matrix is composed of feldspar, quartz, and a small amount of mica. Feldspar is elongated and arranged in a short rod shape with smooth boundaries. The quartz grains are elongated and oriented, the boundary is relatively flat, and the undulose extinction is visible under crossed polarized light (**Figure 3F**). All of the microstructures indicate that feldspar and quartz are flattened and elongated and that they have undergone low-temperature dislocation creep. Scanning electron microscopy shows that quartz grains and small K-feldspar grains are distributed in a strip shape (**Figure 3H**), indicating strong ductile shear deformation.

4.1.2 Electron Backscatter Diffraction Fabric of Quartz for Samples of Mylonite

Quartz fabrics were mapped by EBSD in a total of 10 mylonite thin sections from six samples, and the fabrics of quartz in most thin sections are similar. We present the results of six thin sections from three samples in **Figure 4**. Section 1 (such as Y11-3-1) was cut parallel to the mineral lineation (*X*-axis) and perpendicular to the foliation (*XY* plane) of the mylonites, and section 2 (such as Y11-3-2) was cut perpendicular to *X*-axis and *XY* plane. Grains of quartz, feldspar, and biotite are strongly elongated to form the foliation of mylonite samples, except some phenocrysts of feldspar which display significant plastic deformation for all minerals.

Figure 4 shows the EBSD pole figure of quartz in mylonite samples. The dense concentration of the *c*-axes of quartz grains in samples of Y11-3 (**Figures 4A,B**) and 110829-1 (**Figures 4C,D**) are distributed in the north and south poles, indicating that the slip system is the basal $\langle a \rangle$ slip, which is a typical fabric of low-temperature (below 400°C) deformation, corresponding to bulge creep of quartz. However, the *c*-axes of quartz grains in samples of 110827-2 (**Figures 4E,F**) are distributed in the center point, indicating that the slip system is the prism $\langle a \rangle$ slip, which is a typical fabric of medium-to-high temperature (between 450 and 600°C) deformation. The EBSD results are consistent with the results of microstructural analysis with sub-grain recrystallization creep of quartz. The medium-to-high temperature deformation corresponds to the plastic flow behavior in ductile shear of deep fault zone during the inter-seismic period, while the low-temperature deformation stands for the transient creep of the brittle–plastic transition zone of fault during the inter-seismic period.

4.2 Pseudotachylyte and Cataclasite

4.2.1 Microstructure of Pseudotachylyte and Cataclasite

Samples 110827-3 and Y11-1B are protomylonites overprinted by the cataclasite and pseudotachylyte vein (**Figures 2B,C**). The major minerals of the samples are quartz, feldspar, and biotite

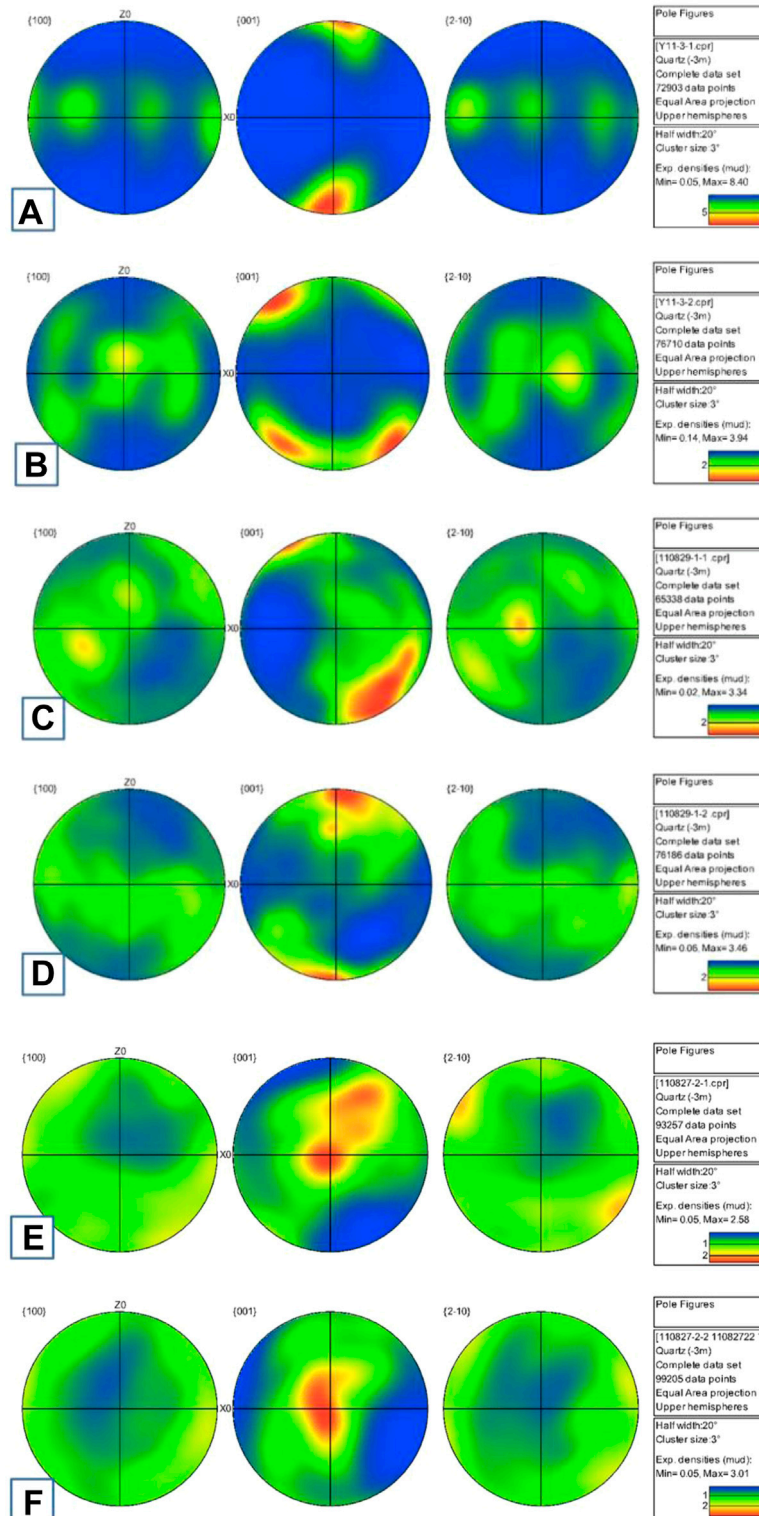


FIGURE 4 | Quartz fabric from EBSD in samples of mylonites. **(A)** Thin section of Y11-3-1, **(B)** thin section of Y11-3-2, **(C)** thin section of 110829-1-1, **(D)** thin section of 110829-1-2, **(E)** thin section of 110827-2-1, and **(F)** thin section of 110827-2-2 (All sections were cut perpendicular to the XY plane of the mylonites, and different numbers -1 or -2 in the same sample were parallel or perpendicular to X-axis).

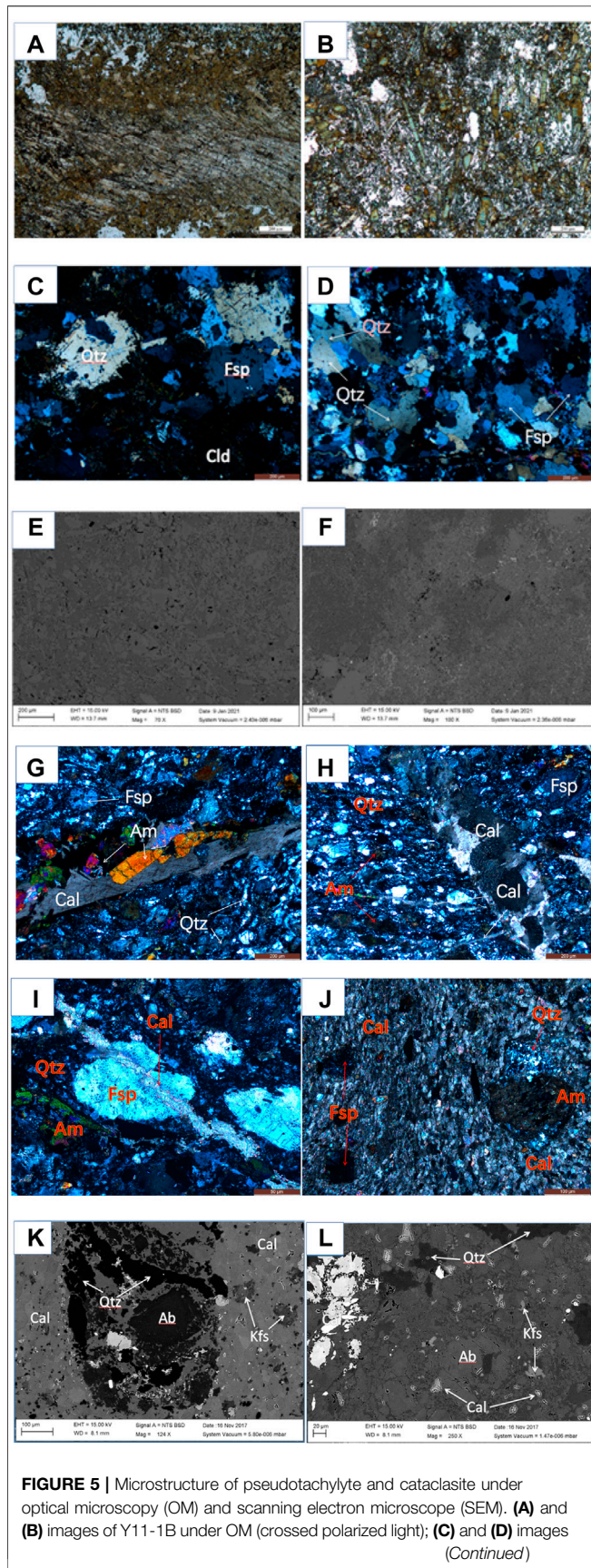
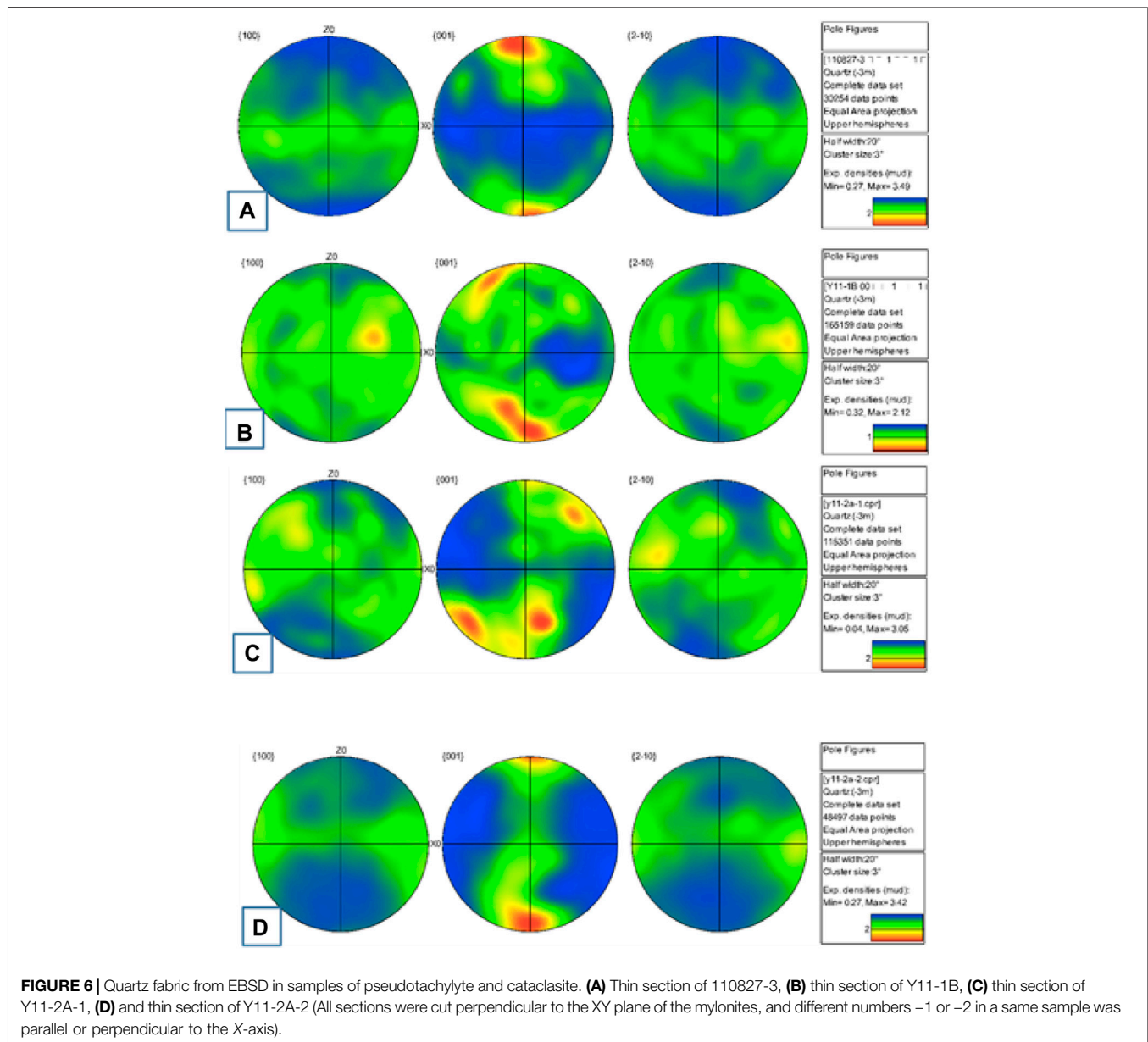


FIGURE 5 | of 110827-3 under OM (crossed polarized light); (E) and (F) images of Y11-1B under SEM; (G), (H), (I), and (J) images of Y11-2A under OM (crossed polarized light); and (K) and (L) images of Y11-2A under SEM. (Qtz, quartz; Fsp, feldspar; Cld, chloritoid; Am, amphibole; Ab, albite; Kfs, K-feldspar; Ca, calcite).

with obvious stretching lineation shown by quartz and biotite. In the hand specimens, the protomylonite was fractured to form cataclasite, and a black vein of pseudotachylyte developed within cataclasite (Figures 2B,C). The boundary between the black vein of pseudotachylyte and wall rock of cataclasite is clear, and the cracks in pseudotachylyte were healed by calcite and sparse pyrite. Sample Y11-2A is a typical cataclasite which is a kind of localized strong cataclastic rock from Y11-1B (Figure 2D), the grains of quartz and feldspar developed mesh-like veins, which were healed by quartz and calcite.

There is a cataclastic zone between the protomylonite and pseudotachylyte vein (Figure 5A). Feldspar grains in cataclasite were fractured, and coarse-grained feldspar developed with mechanical twinning and undulose extinction (Figure 5C) under an optical polarizing microscope. The cracks in feldspar were healed using statically recrystallized quartz and calcite veins, and calcite underwent plastic deformation which represents a post-seismic relaxation deformation. A large number of randomly distributed needle-shaped chloritoid, feldspar, and quartz crystallized in the pseudotachylyte vein (Figures 5B,E,F) which are the products of rapid cooling after co-seismic frictional melting. Two kinds of quartz were found: the first one is semi-automorphic, the boundaries are bulged and recrystallized (Figure 5D), and some grains can be observed as undulose extinction, which is the pre-existing low-temperature deformed quartz in the parent rock; the other one has the characteristics of static recrystallization (Figure 5D in red), which is quartz recrystallized statically from the pseudotachylyte after the rock is broken.

Sample Y11-2A is a typical cataclasite which develops a porphyritic structure, and fractures were healed by calcite veins under a polarized light microscope (Figures 5G–J). The phenocrysts were mostly feldspar grains and altered amphibole. The feldspar grains in the phenocrysts are mostly euhedral to subhedral with irregular grain boundaries generally developing cracks that are filled by calcite veins (Figures 5H,I). The amphibole grains in the phenocrysts are mostly euhedral or subhedral, and there are obvious transcrystalline cracks across the grains. The main components of the matrix are fine-grained feldspar, quartz, and a small amount of mica and amphibole. Fine-grained feldspar and quartz have undulose extinction, and directional elongation shows the characteristics of plastic flow (Figure 5J). The fractures were healed by two types of calcite veins. Among them, the first type of calcite veins is mainly fine-grained aggregates (Figure 5J), which form a band and cuts through the entire cataclasite sample, indicating significant plastic flow. It is speculated that the cracks were produced in the co-seismic slip, were healed by calcite during the post-seismic relaxation period, and then the calcite was plastically deformed under low-temperature condition. The second type of calcite veins is mainly subhedral aggregates, without any deformation



features (Figure 5G), which is the product of carbonate-containing fluid precipitation in the cracks and the slow growth of calcite in the cracks during the later crack-healing stage. Under the scanning electron microscope, it can be observed that the feldspar phenocrysts have crushed cracks (Figures 5K, 5L). The mineral composition and composition variations of the phenocrysts are very complicated. The whole grain is feldspar-shaped (Figure 5K), and the veins are filled with quartz and calcite veins. The matrix of fine-grained feldspar and quartz were cemented with anhedral calcite, plagioclase dissolves into albite, and is partially replaced by amphibole due to reaction with mafic-rich fluid amphibole. These characteristics indicate that the solution and precipitation occurred in the fragmentation of rocks accompanied by the action of fluid after the cataclastic process.

4.2.2 Electron Backscatter Diffraction Fabric of Quartz for Samples of Pseudotachylyte and Cataclasite

All of the pseudotachylyte and cataclasite samples were mapped by EBSD. Images of micro-structures for four sections were given. For pseudotachylyte samples, EBSD analysis focuses on locations of cataclasite beside the pseudotachylyte vein.

In 110827-3 (Figure 6A), the *c*-axes of quartz minerals are distributed in the north and south poles, showing basal $\langle a \rangle$ slip, which is the result of low temperature deformation. In sample Y11-1B (Figure 6B), the *c*-axes of quartz show a dense concentration of intensive areas and no obvious dense concentration. In Y11-2A-1 (Figure 6C), the *c*-axes of quartz are distributed in the north and south poles, showing that the slip system is basal $\langle a \rangle$ slip with low temperature deformation too.

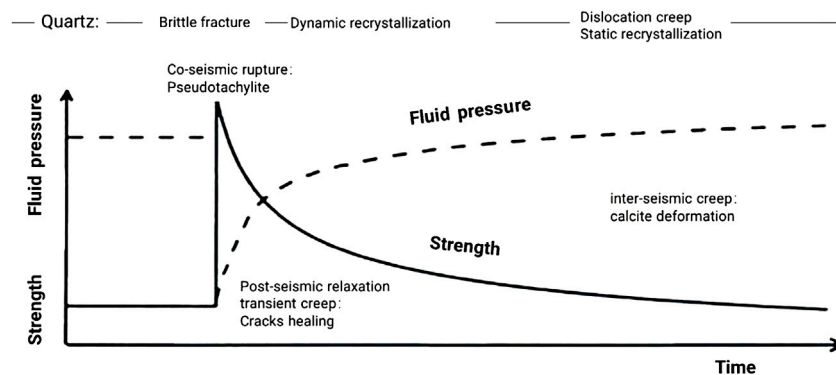


FIGURE 7 | Transient creep model of quartz from co-seismic rupture and post-seismic relaxation to inter-seismic ductile in the brittle-plastic transition of Red River fault (modified from Trepmann and Stöckhert, 2003).

5 DISCUSSION

The dominant sliding system of quartz is the basal sliding, the rhomb sliding, and the prism sliding in turn when the temperature is from low to high or the strain rate is from high to low (Schmid and Casey, 1986; Toy et al., 2008). Under a high-temperature environment, with the increase of the differential stress, the sliding system is the basal $\langle a \rangle$, rhomb $\langle a \rangle$, prism $\langle a \rangle$, and prism $\langle c \rangle$ (Schmid and Casey, 1986; Ji, 1988; Toy et al., 2008; Xia and Liu, 2011). During the ductile deformation of quartz, under the conditions of low temperature (250–400°C), it mainly creeps through the basal $\langle a \rangle$ dislocation slip system; under the conditions of medium temperature (450–600°C), it mainly creeps through the prism $\langle a \rangle$ dislocation slip system; and under high temperature (600–700°C), it mainly creeps through the prism $\langle c \rangle$ dislocation slip system (Schmid and Casey, 1986; Ji, 1988; Heidelbach et al., 2000; Toy et al., 2008; Ábalos et al., 2011). The quartz c -axes pole figure can be used to analyze the slip system inside the crystal to determine its deformation temperature.

The EBSD data show that the slip system of quartz in mylonite samples are basal $\langle a \rangle$ slip and prism $\langle a \rangle$ slip, which display quartz deformed under low-to-medium temperature conditions (250–600°C). EBSD data of quartz in cataclastic samples show basal $\langle a \rangle$ slip only, indicating that the samples deformed under low-temperature deformation environment (250–400°C) which is consistent with Wintsch and Yeh (2013) and Cao et al. (2017). However, EBSD data of quartz in pseudotachylyte does not show an obvious orientation. The EBSD data are consistent with microstructures under optical microscope and SEM.

The medium-to-high temperature deformation of mylonite corresponds to the rheology of ductile layers of the fault zone during the inter-seismic period, while the low-temperature deformation of quartz corresponds to transient creep of the brittle-plastic transition zone of fault. The cataclastic and pseudotachylyte are the results during co-seismic rupture which were superimposed on mylonite. The cracks' healing by quartz and calcite veins in the cataclastic and pseudotachylyte

represents deformation behavior during the post-seismic relaxation period.

Based on microstructures and quartz fabrics of EBSD in this study, we recommend the deformation model of Red River fault for the earthquake period (Figure 7). (1) During the inter-seismic period, the plastic layer in the fault underwent ductile shear deformation to form fine-grained mylonite and ocellar-shaped mylonite; (2) as the stress continued to accumulate, when the stress reached the fault strength, the rocks underwent co-seismic rupture, pseudotachylyte was produced at co-seismic friction slip, and the cataclastic process occurred; (3) and in the subsequent stress relaxation stage, high stress and high strain rate caused feldspar in the rocks to continue to undergo brittle fracture, but fluid filled the cracks which caused healing by quartz and calcite, accompanied by pressure solution. (4) With the gradual stress relaxation, minerals such as quartz and calcite in the cracks transform into static recrystallization, which induced cracks to heal and stress to accumulate; the strength of the fault gradually increases, accumulating energy for the next earthquake.

6 CONCLUSION

Deformation recorded by pseudotachylyte-mylonites in the Red River fault indicates transient creep from inter-seismic ductile to co-seismic rupture. Based on the microstructures and quartz fabrics, we distinguished between different deformations of the brittle-plastic transition zone during the earthquake cycle. (1) Bulge recrystallization with basal $\langle a \rangle$ slip and sub-grain recrystallization with prism $\langle a \rangle$ slip of quartz in samples of mylonite, which are typical fabrics at the low-to-medium temperature dislocation creep, representing inter-seismic ductile shear of fault under the conditions of low stress and low strain rate. (2) *Cataclastic* and pseudotachylyte which were produced by brittle fracture and frictional melting during co-seismic rupture. (3) Crack healing and pressure solution, as well as plastic deformation of calcite, static recrystallization of quartz, and calcite in the veins, which are results of transient creep at the

post-seismic relaxation period. The oscillation deformation model adapted from Trepmann and Stöckhert (2003) could be used to explain transient creep of the brittle–plastic transition zone during the seismic cycle in the Red River fault.

DATA AVAILABILITY STATEMENT

The original contributions presented in the study are included in the article/Supplementary Material, further inquiries can be directed to the corresponding author.

AUTHOR CONTRIBUTIONS

ZY contributed to conception, collection of samples, and design of this study. DW conducted the experiments, DW and ZY wrote the

manuscript. MX guided the use of instruments and discussed the results of SEM and EBSD. All authors contributed to manuscript revision, and read and approved the submitted version.

FUNDING

This research was funded by the National Natural Science Foundation of China (41772223) and National Key Research and Development Project (2018YFC1503404).

ACKNOWLEDGMENTS

We thank prof. Lidong Dai of the Editor and three reviewers for a thoughtful review. We also thank Prof. Changrong He, Prof. Shimamoto, and Prof. Xiaosong Yang for the field works.

REFERENCES

- Ábalos, B., Puelles, P., Fernández-Armas, S., and Sarrionandia, F. (2011). EBSD Microfabric Study of Pre-Cambrian Deformations Recorded in Quartz Pebbles from the Sierra de la Demanda (N Spain). *J. Struct. Geol.* 33, 500–518. doi:10.1016/j.jsg.2011.01.005
- Bestmann, M., Pennacchioni, G., Frank, G., Göken, M., and de Wall, H. (2011). Pseudotachylyte in Muscovite-Bearing Quartzite: Coseismic Friction-Induced Melting and Plastic Deformation of Quartz. *J. Struct. Geol.* 33, 169–186. doi:10.1016/j.jsg.2010.10.009
- Bestmann, M., Pennacchioni, G., Nielsen, S., Göken, M., and de Wall, H. (2012). Deformation and Ultrafine Dynamic Recrystallization of Quartz in Pseudotachylyte-Bearing Brittle Faults: A Matter of a Few Seconds. *J. Struct. Geol.* 38, 21–38. doi:10.1016/j.jsg.2011.10.001
- Brace, W. F., and Kohlstedt, D. L. (1980). Limits on Lithospheric Stress Imposed by Laboratory Experiments. *J. Geophys. Res.* 85, 6248–6252. doi:10.1029/jb085ib11p06248
- Camacho, A., Vernon, R. H., and Fitz Gerald, J. D. (1995). Large Volumes of Anhydrous Pseudotachylyte in the Woodroffe Thrust, Eastern Musgrave Ranges, Australia. *J. Struct. Geol.* 17, 371–383. doi:10.1016/0191-8141(94)00069-c
- Campbell, L. R., and Menegon, L. (2019). Transient High Strain Rate during Localized Viscous Creep in the Dry Lower Continental Crust (Lofoten, Norway). *J. Geophys. Res. Solid Earth* 124, 10240–10260. doi:10.1029/2019jb018052
- Cao, S., Liu, J., Leiss, B., Neubauer, F., Genser, J., and Zhao, C. (2011b). Oligo-Miocene Shearing along the Ailao Shan-Red River Shear Zone: Constraints from Structural Analysis and Zircon U/Pb Geochronology of Magmatic Rocks in the Diancang Shan Massif, SE Tibet, China. *Gondwana Res.* 19, 975–993. doi:10.1016/j.gr.2010.10.006
- Cao, S., Liu, J., Leiss, B., Vollbrecht, A., Genser, J., Neubauer, F., et al. (2012). Initiation of Left-Lateral Deformation along the Ailao Shan-Red River Shear Zone: New Microstructural, Textural, and Geochronological Constraints from the Diancang Shan Metamorphic Massif, SW Yunnan, China. *Int. Geol. Rev.* 54, 348–367. doi:10.1080/00206814.2010.543789
- Cao, S., Neubauer, F., Liu, J., Bernroider, M., Cheng, X., Li, J., et al. (2017). Rheological Weakening of High-Grade Mylonites during Low-Temperature Retrogression: The Exhumed Continental Ailao Shan-Red River Fault Zone, SE Asia. *J. Asian Earth Sci.* 139, 40–60. doi:10.1016/j.jseae.2016.10.002
- Cao, S., Neubauer, F., Liu, J., Genser, J., and Leiss, B. (2011a). Exhumation of the Diancang Shan Metamorphic Complex along the Ailao Shan-Red River Belt, Southwestern Yunnan, China: Evidence from $40\text{Ar}/39\text{Ar}$ Thermochronology. *J. Asian Earth Sci.* 42, 525–550. doi:10.1016/j.jseae.2011.04.017
- Chernak, L. J., Hirth, G., Selverstone, J., and Tullis, J. (2009). Effect of Aqueous and Carbonic Fluids on the Dislocation Creep Strength of Quartz. *J. Geophys. Res.* 114, B04201. doi:10.1029/2008jb005884
- Cowan, D. S. (1999). Do faults Preserve a Record of Seismic Slip? A Field Geologist's Opinion. *J. Struct. Geol.* 21, 995–1001. doi:10.1016/s0191-8141(99)00046-2
- Dai, W. H., and Zhou, Y. S. (2019). Deformation of the Brittle-Plastic Transition Zone at the Post-Seismic Relaxation Period: A Case Study of the Red River Fault. *Seismol. Geol.* 41 (4), 996–1011. doi:10.3969/j.issn.0253-4967.2019.04.012 (in Chinese with English Abstract)
- Gueydan, F., Leroy, Y. M., and Jolivet, L. (2004). Mechanics of Low-Angle Extensional Shear Zones at the Brittle-Ductile Transition. *J. Geophys. Res.* 109, B12407. doi:10.1029/2003jb002806
- Heidelbach, F., Kunze, K., and Wenk, H.-R. (2000). Texture Analysis of a Recrystallized Quartzite Using Electron Diffraction in the Scanning Electron Microscope. *J. Struct. Geol.* 22 (1), 91–104. doi:10.1016/s0191-8141(99)00125-x
- Hobbs, B. E., Ord, A., and Teyssier, C. (1986). Earthquakes in the Ductile Regime? *Pure Appl. Geophys.* 124, 309–336. doi:10.1007/bf00875730
- Ikari, M. J., Niemeijer, A. R., and Marone, C. (2011). The Role of Fault Zone Fabric and Lithification State on Frictional Strength, Constitutive Behavior, and Deformation Microstructure. *J. Geophys. Res.* 116, B08404. doi:10.1029/2011JB008264
- Ji, S. C. (1988). Dislocation Splitting in Main Rock-Forming Minerals and its Rheological Implications. *Geoscience* 1988 (4), 118–125. (in Chinese with English Abstract)
- Kim, J.-W., Ree, J.-H., Han, R., and Shimamoto, T. (2010). Experimental Evidence for the Simultaneous Formation of Pseudotachylyte and Mylonite in the Brittle Regime. *Geology* 38, 1143–1146. doi:10.1130/G31593.1
- Kohlstedt, D. L., Evans, B., and Mackwell, S. J. (1995). Strength of the Lithosphere: Constraints Imposed by Laboratory Experiments. *J. Geophys. Res.* 100 (B9), 17587–17602. doi:10.1029/95jb01460
- Leloup, P. H., and Kienast, J.-R. (1993). High-Temperature Metamorphism in a Major Strike-Slip Shear Zone: The Ailao Shan-Red River, People's Republic of China. *Earth Planet. Sci. Lett.* 118, 213–234. doi:10.1016/0012-821x(93)90169-a
- Leloup, P. H., Lacassin, R., Tapponnier, P., Schärer, U., Zhong, D., Liu, X., et al. (1995). The Ailao Shan-Red River Shear Zone (Yunnan, China), Tertiary Transform Boundary of Indochina. *Tectonophysics* 251, 3–84. doi:10.1016/0040-1951(95)00070-4
- Li, W., Cao, S., Zhan, L., Cheng, X., Li, W., and Lyu, M. (2022). Crush-Origin Pseudotachylyte in Granitic Mylonites of Continental Exhumed Ailaoshan-Red River Shear Zone Southeastern Asia. *J. Struct. Geol.* 159, 104606. doi:10.1016/j.jsg.2022.104606
- Lin, A., Maruyama, T., Aaron, S., Michibayashi, K., Camacho, A., and Kano, K.-I. (2005). Propagation of Seismic Slip from Brittle to Ductile Crust: Evidence from Pseudotachylyte of the Woodroffe Thrust, Central Australia. *Tectonophysics* 402, 21–35. doi:10.1016/j.tecto.2004.10.016
- Liu, J. L., Wang, A. J., Cao, S. Y., Zou, Y. X., Tang, Y., and Chen, Y. (2008). Geochronology and Tectonic Implication of Migmatites from Diancangshan, Western Yunnan, China. *Acta Petrol. Sin.* 24, 413–420. doi:10.1016/j.sedgeo.2008.02.002

- Liu, Y. P., Ye, L., Li, C. Y., Song, B., Li, T. S., Guo, L. G., et al. (2006). Discovery of the Neoproterozoic Magmatism in Southeastern Yunnan: Evidence from SHRIMP Zircon U–Pb Dating and Litho geochemistry. *Acta Petrol. Sin.* 22, 916–926. doi:10.1016/j.sedgeo.2005.11.021
- McKenzie, D., and Brune, J. N. (1972). Melting on Fault Planes during Large Earthquakes. *Geophys. J. Int.* 29, 65–78. doi:10.1111/j.1365-246x.1972.tb06152.x
- Moecher, D. P., and Steltenpohl, M. G. (2009). Direct Calculation of Rupture Depth for an Exhumed Paleoseismogenic Fault from Mylonitic Pseudotachylyte. *Geology* 37, 999–1002. doi:10.1130/G30166A.1
- Molnar, P., and Tapponnier, P. (1975). Cenozoic Tectonics of Asia: Effects of a Continental Collision: Features of Recent Continental Tectonics in Asia Can Be Interpreted as Results of the India-Eurasia Collision. *Science* 189 (4201), 419–426. doi:10.1126/science.189.4201.419
- Molnar, P., and Tapponnier, P. (1977). Relation of the Tectonics of Eastern China to the India-Eurasia Collision: Application of Slip-Line Field Theory to Large-Scale Continental Tectonics. *Geology* 5 (4), 212–216. doi:10.1130/0091-7613(1977)5<212:rottoe>2.0.co;2
- Montési, L. G. J., and Zuber, M. T. (2002). A Unified Description of Localization for Application to Large-Scale Tectonics. *J. Geophys. Res.* 107, ECV1.1–ECV1.21. doi:10.1029/2001JB000465
- Nevitt, J. M., Warren, J. M., and Pollard, D. D. (2017). Testing Constitutive Equations for Brittle-Ductile Deformation Associated with Faulting in Granitic Rock. *J. Geophys. Res. Solid Earth* 122, 6269–6293. doi:10.1002/2017JB014000
- Papa, S., Pennacchioni, G., Menegon, L., and Thielmann, M. (2020). High-Stress Creep Preceding Coseismic Rupturing in Amphibolite-Facies Ultramylonites. *Earth Planet. Sci. Lett.* 541, 116260. doi:10.1016/j.epsl.2020.116260
- Passchier, C. W. (1982). Pseudotachylyte and the Development of Ultramylonite Bands in the Saint-Barthélemy Massif, French Pyrenees. *J. Struct. Geol.* 4, 69–79. doi:10.1016/0191-8141(82)90008-6
- Pennacchioni, G., and Cesare, B. (1997). Ductile-Brittle Transition in Pre-Alpine Amphibolite Facies Mylonites during Evolution from Water-Present to Water-Deficient Conditions (Mont Mary Nappe, Italian Western Alps). *J. Metamorph Geol.* 15, 777–791. doi:10.1111/j.1525-1314.1997.00055.x
- Pennacchioni, G., Di Toro, G., Brack, P., Menegon, L., and Villa, I. M. (2006). Brittle-Ductile-Brittle Deformation during Cooling of Tonalite (Adamello, Southern Italian Alps). *Tectonophysics* 427, 171–197. doi:10.1016/j.tecto.2006.05.019
- Schmid, S. M., and Casey, M. (1986). Complete Fabric Analysis of Some Commonly Observed Quartz C-Axis Patterns. *Geophys Monogr.* 36, 263–286. doi:10.1029/gm036p0263
- Scholz, C. H. (1988). The Brittle-Plastic Transition and the Depth of Seismic Faulting. *Geol. Rundsch.* 77, 319–328. doi:10.1007/bf01848693
- Sibson, R. H. (1983). Continental Fault Structure and the Shallow Earthquake Source. *J. Geol. Soc.* 140, 741–767. doi:10.1144/gsjgs.140.5.0741
- Sibson, R. H. (1975). Generation of Pseudotachylyte by Ancient Seismic Faulting. *Geophys J. Int.* 43, 775–794. doi:10.1111/j.1365-246x.1975.tb06195.x
- Sibson, R. H. (1980). Transient Discontinuities in Ductile Shear Zones. *J. Struct. Geol.* 2, 165–171. doi:10.1016/0191-8141(80)90047-4
- Song, B. R., Johnson, S. E., Song, W. J., Gerbi, C. C., and Yates, M. G. (2020). Coseismic Damage Runs Deep in Continental Strike-Slip Faults. *Earth Planet. Sci. Lett.* 539, 116226. doi:10.1016/j.epsl.2020.116226
- Takagi, H., Goto, K., and Shigematsu, N. (1999). Ultramylonite Bands Derived from Cataclasite and Pseudotachylyte in Granites, Northeast Japan. *J. Struct. Geol.* 22, 1325–1339.
- Tapponnier, P., Peltzer, G., and Armijo, R. (1986). On the Mechanics of the Collision between India and Asia. *Geol. Soc. Spec. Publ.* 19, 115–157. doi:10.1144/gsl.sp.1986.019.01.07
- Tapponnier, P., Peltzer, G., Le Dain, A. Y., Armijo, R., and Cobbold, P. (1982). Propagating Extrusion Tectonics in Asia: New Insights from Simple Experiments with Plasticine. *Geology* 10, 611–616.
- Toy, V. G., David, J. P., and Richard, J. N. (2008). Quartz Fabrics in the Alpine Fault Mylonites: Influence of Pre-Existing Preferred Orientations on Fabric Development during Progressive Uplift. *J. Struct. Geol.* 30, 602–621. doi:10.1016/j.jsg.2008.01.001
- Trepmann, C. A., Hsu, C., Hentschel, F., Döhler, K., Schneider, C., and Wichmann, V. (2017). Recrystallization of Quartz after Low-Temperature Plasticity - The Record of Stress Relaxation below the Seismogenic Zone. *J. Struct. Geol.* 95, 77–92. doi:10.1016/j.jsg.2016.12.004
- Trepmann, C. A., Stöckhert, B., Dorner, D., Moghadam, R. H., Küster, M., and Röller, K. (2007). Simulating Coseismic Deformation of Quartz in the Middle Crust and Fabric Evolution during Postseismic Stress Relaxation - An Experimental Study. *Tectonophysics* 442, 83–104. doi:10.1016/j.tecto.2007.05.005
- Trepmann, C. A., and Stöckhert, B. (2003). Quartz Microstructures Developed during Non-Steady State Plastic Flow at Rapidly Decaying Stress and Strain Rate. *J. Struct. Geol.* 25, 2035–2051. doi:10.1016/s0191-8141(03)00073-7
- Trepmann, C. A., and Stöckhert, B. (2013). Short-Wavelength Undulatory Extinction in Quartz Recording Coseismic Deformation in the Middle Crust - an Experimental Study. *J. Geophys. Res. Solid Earth* 4, 263–276. doi:10.5194/se-4-263-2013
- Tse, S. T., and Rice, J. R. (1986). Crustal Earthquake Instability in Relation to the Depth Variation of Frictional Slip Properties. *J. Geophys. Res.* 91, 9452–9472. doi:10.1029/jb091ib09p09452
- Tullis, J., and Yund, R. (1992). “Chapter 4 the Brittle-Ductile Transition in Feldspar Aggregates: An Experimental Study,” in *Fault Mechanisms and Transport Properties of Rocks*. Editors B. Evans and T.-F. Wong (New York: Academic Press), 89–117. doi:10.1016/s0074-6142(08)62816-8
- White, J. C. (2012). Paradoxical Pseudotachylyte - Fault Melt outside the Seismogenic Zone. *J. Struct. Geol.* 38, 11–20. doi:10.1016/j.jsg.2011.11.016
- White, J. C. (1996). Transient Discontinuities Revisited: Pseudotachylyte, Plastic Instability and the Influence of Low Pore Fluid Pressure on Deformation Processes in the Mid-Crust. *J. Struct. Geol.* 18, 1471–1486. doi:10.1016/s0191-8141(96)00059-4
- Wintsch, R. P., and Yeh, M.-W. (2013). Oscillating Brittle and Viscous Behavior through the Earthquake Cycle in the Red River Shear Zone: Monitoring Flips between Reaction and Textural Softening and Hardening. *Tectonophysics* 587, 46–62. doi:10.1016/j.tecto.2012.09.019
- Xia, H. R., and Liu, J. L. (2011). The Crystallographic Preferred Orientation of Quartz and its Applications. *Geol. Bull. China* 30 (1), 58–70. doi:10.3969/j.issn.1671-2552.2011.01.006 (in Chinese with English Abstract)
- Zhou, Y. S., Han, L., Jing, C., He, C.-R., and Dang, J. (2014). The Rheological Structures of Brittle-Plastic Transition in Longmenshan Fault Zone and Seismogenic Mechanism of Wenchuan Earthquake. *Seismol. Geol.* 36 (3), 882–895. (in Chinese with English Abstract). doi:10.3969/j.issn.0253-4967.2014.03.025

Conflict of Interest: The authors declare that the research was conducted in the absence of any commercial or financial relationships that could be construed as a potential conflict of interest.

Publisher's Note: All claims expressed in this article are solely those of the authors and do not necessarily represent those of their affiliated organizations, or those of the publisher, the editors, and the reviewers. Any product that may be evaluated in this article, or claim that may be made by its manufacturer, is not guaranteed or endorsed by the publisher.

Copyright © 2022 Dai, Zhou and Ma. This is an open-access article distributed under the terms of the Creative Commons Attribution License (CC BY). The use, distribution or reproduction in other forums is permitted, provided the original author(s) and the copyright owner(s) are credited and that the original publication in this journal is cited, in accordance with accepted academic practice. No use, distribution or reproduction is permitted which does not comply with these terms.